Turbulent channel flow tests

June 29, 2018

List of Figures

List of Tables

Nomenclature

Latin symbols

$\bar{u}$	filtered stream-wise velocity
$\bar{v}$	filtered wall-normal velocity
$\bar{w}$	filtered span-wise velocity
U	Mean stream-wise velocity
u	stream-wise velocity fluctuation
V	Mean wall-normal velocity
v	wall-normal velocity fluctuation
W	Mean span-wise velocity
w	span-wise velocity fluctuation
L_x	Length of the domain, stream-wise direction
L_y	Height of the domain, wall-normal direction
L_z	Width of the domain, span-wise direction

Greek symbols

$\mathbb{H}$	Quaternions
$\mathbb{C}$	Complex Numbers
$\mathbb{R}$	Real Numbers
δ	Half-channel height, wall-normal direction

Brackets, Superscripts, Sub-scripts

ρ	Friction Index
V	Constant Volume

Contents

1 Introduction

1.1 Literature survey

1.2 Objectives and Motivation

2 Lattice Boltzmann theories

2.1 BGK

2.2 MRT

2.3 Cumulant LBM

3 Turbulence theories

i DNS.
Direct numerical simulation (DNS) method uses a modelling-free approach for approximation of the exact solution, as the navier-stokes equation comprises of all turbulence mechanisms. Since the turbulence is three dimensional and inherently instationary it has to take in to account all the components present in the navier stokes equation.Turbulence involves the interaction in between the scales of various different sizes and thus to represnt the exact solution or the characteristics of the turbulent flow considered correctly, the DNS method emphasises on the fine spatial and temporal resolution of the meshes. Apart from that this method requires the discretization methods to have low level of numerical dissipation and dispersion. In order to correctly determine the effects of the turbulence intensity, the fluctuating flow variables which satisfy the navier stokes equation are provided as inputs.
ii DES.
Detached eddy simulation, DES, combines the approach of RANS and the LES method; it therefore belongs to the class of the hybrid RANS-LES simulations. The basic idea of this method is that the near wall boundary layer would be resolved using the RANS approach, while the usuage of LES to (correctly) resolve such regions requires a very fine spatial and temporal resolution, as the turbulent scales to be resolved in the boundary layers are very small. On the other hand, the detached regions, wakes and the free shear layers are the regions, where the RANS model frequently fails, are handled by the LES.

DES was first introduced by *Spalart et al.*. The goal was to compute the aerodynamic flows involving massive seperation with a moderate increase in the grid resolution compared to the RANS method. The idea behind the DES is to segregate the flow, using suitable detectors, in to the domains where the entire energy spectrum will be modelled using the RANS (near wall boundary layer) or the large energy containing structures are resolved using the LES method (detached flow region). Therefore in this approach, a suitable method is chosen, for each domain, in terms of efficiency and accuracy.

In comparison with LES, for the computation of the flows involving the boundary layer, DES reduces the computational effort significantly. Since the flows involved are unsteady and three dimensional turbulent flows, the computational effort will be relatively higher when compared with RANS.

Avery good compilation of the hybrid RANS-LES approach is found in *Fröhlich and von Tersi (2008)*

3.1 RANS

3.2 LES

4 Implementation

4.1 Discretisation

4.2 Implementation of eddy viscosity contribution

4.3 Taylor-Green vortex simulations

5 Model set-up and theories

Apart from the free shear flows, most turbulent flows are bounded by one or more solid surfaces depending on whether they belong to class of the internal or external flow of fluids i.e. flow through pipes and flow over a car respectively. In this investigation one of the simplest internal flow has been chosen for the validation & testing of the implementation: fully developed channel flow. This flow is considered to be of prime importance as it has played a prominent role in the development of the study of the wall bounded turbulent flows [3]. [3] has described the fundamental theories of the full developed channel flow in great detail. [4] also has a good compilation on the fully developed channel flow.

In this section a brief description of the turbulent channel flow with some basic theories is presented. Later on it is followed by description of the computational domain, meshing, initial conditions, boundary conditions, pressure gradient modelling, solver settings and in the end by post-processing.

5.1 Turbulent channel flow

Fully developed turbulent channel flow is a classic benchmark case and has been studied extensively to investigate and understand the mechanics of wall-bounded turbulent flows. It is the geometrical simplicity of this case that has lured to a large number of, computational (DNS) and experimental, investigations being carried out for the turbulent channel flow over the years and as a result, an adequate database (DNS data) for certain Re-numbers is already available [5]. Historical progression in the turbulent channel flow simulations have been very well documented in the literature by *Kim et al.* [6]. Also, Kim has pointed out several difficulties related to the experimental measurements and how numerical simulations serve as an essential tool, alongside the experimental results, for the study of the wall-bounded turbulence. The recent development along with the comparison of the DNS results of the turbulent channel flow simulations for higher Re-numbers is documented in [7].

As shown in figure 1, a 3D rectangular duct has been chosen as the compu-

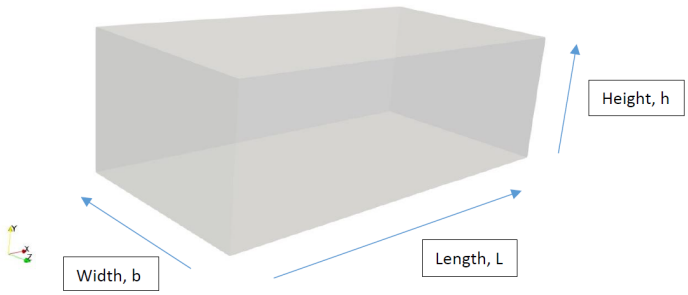

Figure 1: 3D rectangular duct

tational domain. The positive x-axis is the stream-wise direction or the flow direction with the flow varying in the y-direction, the height $h = 2\delta$, the wall-

normal direction. The z-axis is the span-wise direction, the width b. The domain is long and has a large aspect ratio ($b/\delta \gg 1$). The bottom (y = 0) and top (y = 2δ) surfaces of the domain are walls. The mid-plane (y = δ), which is frequently termed as the half-channel width in the literature, is ambiguous with the assigned Cartesian coordinate directions in this case and hence term half-channel height will be used(h = δ).

The mean velocities in the three directions are U, V, W, the stream-wise, wall-normal and span-wise velocities, and the corresponding fluctuating velocities are u,v and w. The mean span-wise or cross-stream velocity is zero, $W = 0$. In the turbulent channel flow test case, fully developed flow region in the channel is of our interest i.e. it is the region where the velocity statistics of the flow remain invariant to spatial changes, x-direction in our case. Also, the domain is large enough in the span-wise direction, z, compared to the half-channel height, δ, so that the flow remains statistically independent of the z-direction. In short, we have two homogeneous flow directions along x & z-axis. Thus, the flow is said to be statistically one- dimensional as the flow statistics vary only in one-direction i.e. y-direction.

5.1.1 Governing equations

Turbulent channel flow is fully developed, where the velocity statistics along the stream-wise direction remain constant i.e. $\partial U/\partial x = 0$, and statistically one dimensional, where the flow statistics vary only in the wall-normal(y) direction. There is no mean flow in the span-wise direction i.e $W = 0$ and thus the gradient of the span-wise velocity in the span-wise direction is zero i.e. $\partial W/\partial z = 0$. The mean continuity equation for the incompressible flow results in the mean wall normal velocity gradient to be zero:

$$\partial V/\partial y = 0 \tag{1}$$

The eq. 1 when integrated, within the wall limits [0,2δ], gives $V = const(y)$ and using the no-slip boundary condition, $U_i = 0$, applied at the walls results in $V = 0$. Now to satisfy the resulting continuity equation eq. 1, V has to be zero everywhere in the domain. Using the above made considerations and applying it to the mean stream-wise momentum equation we will have the following force balance:

$$\frac{\partial \tau}{\partial y} = \frac{\partial P}{\partial x} \tag{2}$$

where $\tau = \left(\mu \frac{\partial U}{\partial y} - \rho \overline{u_i u_j}\right)$ is the total shear stress.

The eq. 2 shows that the total shear stress gradient and the pressure gradient balance each other in the full developed channel flow. It shows an equality of the form *f(x) = g(y)* and for this equality to hold it is important that both *f(x)* and *g(y)* are individually constants. In eq. 2 both the gradients are dependent on different variables and thus they must be individually constants for this equality to hold.

$$\frac{\partial P}{\partial x} = const \;\&\; \frac{\partial \tau}{\partial y} = const$$

Total shear stress is the summation of the viscous stress, $\mu \frac{\partial U}{\partial y}$, and the Reynolds

stress, $-\rho\overline{u_i u_j}$. At the wall with the no-slip boundary condition applied, the Reynolds stresses are reduced to zero and thus the shear stress near the wall or to be specific at the wall would entirely be dominated by the viscous stresses. At the walls the Reynolds stresses drop to zero and the stress at the walls can be defined as the *wall shear stress*, the region where the viscous stresses are dominant:

wall shear stress

$$\begin{aligned} \tau_w &= \mu \frac{\partial U}{\partial y} \\ \tau(0) = \tau_w &= -\tau(2\delta) \end{aligned} \tag{3}$$

Now we can integrate the eq. 2, from 0 to 2δ, for the pressure gradient and express the solution in terms of the τ_w:

$$-\frac{\partial P}{\partial x} = \frac{\tau_w}{\delta} \ , \tag{4}$$

From the fully developed channel flow it is known that the mean velocity profile (time-averaged) remains constant. It is clear from eq. 3 that wall shear stress is linearly proportional to the velocity gradient near the wall. A constant velocity profile implies that the wall shear stress will also be constant in a fully developed channel flow. Thus from eq.4 we can say that the pressure gradients is constant. Integrating the eq. 2, from 0 to some y, with the no-slip boundary condition at the wall results in the following solution:

$$\tau(y) = \tau_w \left(1 - \frac{y}{\delta}\right) \tag{5}$$

It is this pressure gradient that drives the flow through the infinite parallel plates.The pressure gradient in eq. 4 is negative as the viscous effects decreases the pressure along the stream-wise direction. For a given pressure gradient and the half-channel height we get a linear shear stress profile from eq. 4 and 5 independent of the fluid properties and the state of the fluid motion (laminar or turbulent) [3]. Experimental and numerical results [6] show that the total shear stress profile is anti-symmetric about the channel mid height $y = \delta$ and thus $\tau(\delta) = 0$.

5.1.2 Scaling units

The Reynolds stresses decreases towards the wall, remain zero at the wall and so does the eddy viscosity (*Boussinesq hypothesis*). The value of the eddy viscosity ranges from zero, at the wall, to several orders of magnitude higher than the molecular viscosity, in the core region of the turbulent boundary layer [1]. From the figure. 2 it can be seen that the velocity profile changes more slowly (more flatter compared to the parabolic flow profile) in the core of the turbulent boundary layer, where the eddy viscosity is higher than the molecular viscosity, and there is an abrupt change in the velocity profile near the wall, where the molecular viscosity is dominant. The turbulent flow profile has the largest gradient near the wall.

Turbulent flow along the wall can be considered to consist of four different layers, characterised by their distance from the wall. All four layers have been

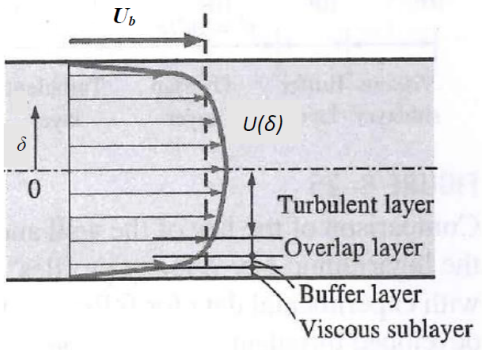

Figure 2: Velocity profile in the fully developed channel flow [1]

approximately shown in figure 2. The layer closet to the wall is the viscous sub-layer, where the viscous effects are dominant. The velocity profile changes linearly with the distance from the wall and the flow is streamlined. Next to the viscous sub-layer is the buffer layer, where the turbulent stresses start to develop, but still the viscous stresses are dominant. Above the buffer layer is the overlap layer, where the turbulent stresses are significant, but still not dominant enough as the viscous stresses. The layer above the overlap layer for the rest of the flow is the outer or turbulent layer, where the turbulence stresses dominate over the viscous stresses.
A single analytical relation for the entire turbulent velocity profile is not suitable, as different regions or layers execute different flow characteristics. The best possible option is to find the key parameters or the functional forms using the dimensional analysis and later on experimental data can be used to obtain the numerical values of the any constants.

i. Viscous sub-layer : With the no-slip boundary condition applied at the wall, $u_i(0,t) = 0$, the entire contribution to the shear stress is purely via viscous stresses i.e. τ_w. From eq. 3 it is clear that shear stress is proportional to the molecular viscosity. The thickness of this layer is very small, but it plays an important role on the flow characteristic because of the presence of large velocity gradients in it. The velocity profile remains linear in this layer and also it has been shown in certain experiments [1]. Since the velocity profile is linear the gradient in the equation 3 remains constant i.e. $\partial U/\partial y = U/y$. Thus the wall shear stress can be written as:

$$\frac{\tau_w}{\rho} = \frac{\nu U}{y} \tag{6}$$

Near the wall the important parameters are : τ_w, ρ, ν. The square root of the term on the left hand side has the dimensions of velocity and thus we define a new parameter as the ***friction velocity***, u_τ:

$$u_\tau = \sqrt{\frac{\tau_w}{\rho}} \tag{7}$$

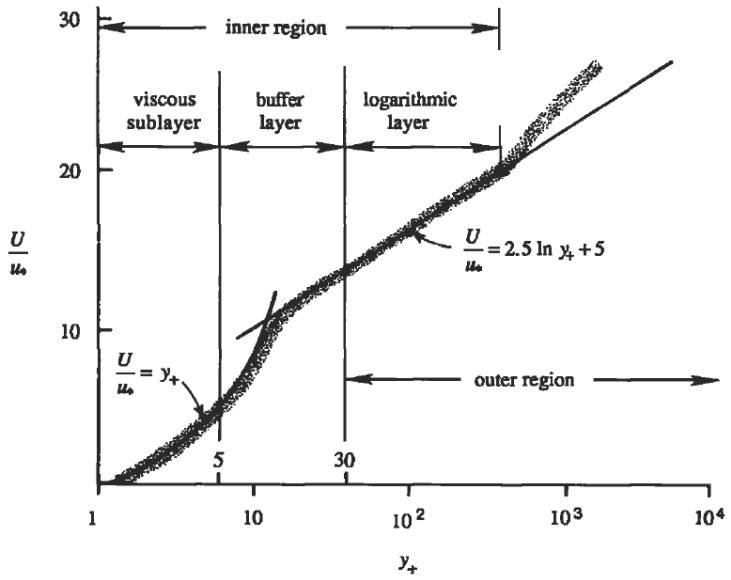

Figure 3: Nondimensional velocity u^+ vs. the nondimensional distance y^+ (plotted in logarithmic scale) [2]

Replacing u_τ in the eq. 6 we have ***the law of wall***:

$$\frac{U}{u_\tau} = \frac{u_\tau y}{\nu} \tag{8}$$

The quantity ν/u_τ has the dimensions of length and it is called ***viscous length*** , δ_ν, and it is used to nondimensionalze the distance from the wall, y. In the analysis of the boundary layer flow, it is convenient to work with the nondimensionalised distance and the velocity. The nondimensionalised quantities are represented with a +.

Nondimensionalised variables :

$$y^+ = \frac{yu_\tau}{\nu} \; and \; u^+ = \frac{U}{u_\tau} \tag{9}$$

Normalised law of the wall :

$$u^+ = y^+ \tag{10}$$

This law shows a very good correlation with the experimental data for smooth surfaces for $0 \leq u_\tau y/\rho \leq 5$. Thus for the $y^+ = 5$ we will have the linear velocity profile in the viscous sub-layer.

ii. Overlap layer: From the dimensional analysis and the experimental results it proved that the velocity in the overlap region is proportional to the logarithm of distance and it can be expressed as:

$$u^+ = \frac{1}{\kappa} \; ln \; y^+ + \; B \; or \; u^+ = 2.5 \; ln \; y^+ + \; 5.0 \tag{11}$$

where κ and B are constants and equal to 0.40 and 5.0 respectively. The eq. 11 is called the *logarithmic law* and the overlap layer is also called as the *logarithmic layer* or *log-law layer*. It is clear from the figure 3 that the eq. 11 represents the experimental data quite satisfactorily from $y^+ \geq 30$ till outer region. Neither eq. 11 nor the eq. 8 represents the experimental data satisfactorily in the buffer layer. From Figure. 3 it is seen that :

viscous sub-layer : $y^+ \leq 5$

buffer layer : $y^+ \geq 5$ till $y^+ \leq 30$

logarithmic layer : $y^+ \geq 30$ till $y^+ \leq 10^3$

iii. Outer layer: The velocity law for this region is:

$$\frac{(U_{max} - U)}{u_\tau} = \frac{1}{\kappa}\ ln\ \left(\frac{y}{\delta}\right) \tag{12}$$

The difference between the mean center line velocity, U_{max}, and the mean velocity, U is called the ***velocity defect*** and thus this law is called the ***velocity defect-law***. In this region the turbulent stresses are dominant compared to the viscous stresses and this is also seen from the eq. 12: the normalised velocity profile in the core region of the turbulent channel flow is dependent on the half-channel height and is not dependent on the viscosity.

5.2 Reynolds number

Since the Reynolds number is used to characterize the flow, great care was taken to simulate the same flows i.e. same Reynolds number as that of the DNS data was used. The dimensionless Reynolds number requires three parameters for its definition: characteristics length (δ), characteristic velocity (V_{ch}) and the kinematic viscosity (ν) of the fluid.

$$Re = \frac{V_{ch}\delta}{\nu}$$

Several choices of V_{ch} are possible, but in this investigation two different V_{ch} have been chosen and the respective Reynolds number are as follows :

i. Friction Reynolds number (Re_τ):

$$Re_\tau = \frac{u_\tau \delta}{\nu} = \frac{\delta}{\delta_\nu} \tag{13}$$

ii. Bulk Reynolds number (Re_b):

$$Re_b = \frac{U_b\ 2\delta}{\nu} \tag{14}$$

The bulk mean velocity is defined as:

$$U_b = \frac{1}{h}\int_0^h U dy$$

5.3 Computational Domain and Meshing

5.3.1 Computational Domain

We are interested to investigate the fully developed turbulent channel and that implies a sufficient length and width of the domain for the flow in the channel to be fully developed. Since the stream-wise and the span-wise directions are homogeneous, periodic boundary conditions are applied on either side of the two homogeneous directions. All flow properties along with the state of the flow are set to be equal for the equivalent points on the periodic boundary pairs. Use of periodic boundaries is equivalent to having an infinitely long domain in that direction. This implies that we have a flow between two infinite parallel planes, Figure 4. Since the artificial periodic boundaries are enforced great care

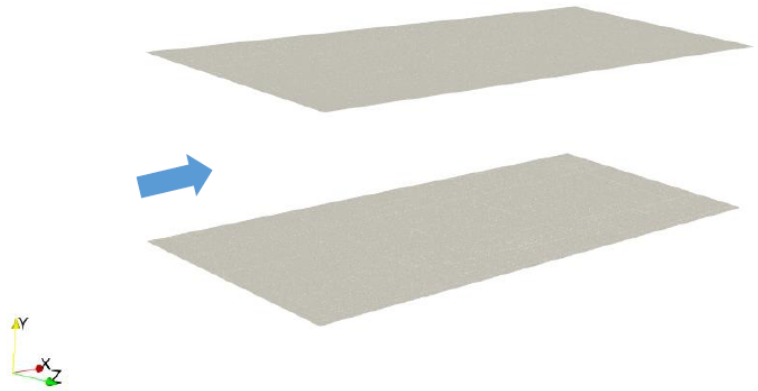

Figure 4: Flow between the infinite parallel plates

has to be taken that the domain is long enough to avoid this artificial boundary conditions from influencing the results.*Moin et.al* [8] has specified certain aspects to be considered in the process of choosing the dimensions of the flow domain for the numerical simulation of the turbulent channel flow. According to [8] the experimental two-point correlation functions have to be considered for choosing the stream-wise (L_x) and the span-wise (L_z) lengths. The usage of periodic boundary conditions is justified if the distance between the pair of periodic boundaries is at least twice the distance, at which the correlation function becomes zero. This means that the domain size is enough to accommodate the largest eddy without the pair of periodic boundaries influencing each other.

To validate the LES results of the fully developed turbulent channel flow the DNS data from the database of [9] for the $Re_\tau = 395$ is used. The authors have shown the adequacy of the domain by performing the two-point spatial correlations. Same domain size used in [9] has been chosen for performing the LES of channel flow, Table 1. Thus, no separate study for two-point correlation has been performed in this investigation.
Several authors [10, 11] have performed the turbulent channel flow simulations with smaller domain dimensions comapred to the dimensions used in the refer-

$Nominal Re_\tau$	L_x x L_yx L_z
395	$2\pi\delta$ x 2δ x $\pi\delta$

Table 1: The size of the domain in x, y, z directions

ence data, [9], in order to either save the computational time or to statiate the upper limit of the total gird points on a Graphic card [11]. But *Bespalko* [12] suggests that for performing the validation studies the dimensions of the domain should be similar to that used in the reference data. Else, the usage of smaller domain dimensions might add some kind of error and this might be than attributed to the error originating from the implementation under test.

5.3.2 Physical parameters

The physical parameters that are necessary for the model set-up and later on for the simulations are pressure gradient(to drive the flow), discussed in the later section, u_τ, ν and U_b In [9] the authors have not specified u_τ, ν and U_b used in the simulations. [13] has computed and specified these parameters obtained from the DNS results of [9] for $Re_\tau = 395$, Table 2 :

Physical quantity	*Value in S.I Units*
Half channel height, δ	1.0 m
Friction velocity, u_τ	0.0079 m/s
Bulk velocity, U_b	0.1335 m/s
Kinematic Viscosity, ν	0.00002 m^2/s

Table 2: Physical quantities

In order to compute the bulk mean velocity from the DNS data (Mean stream-wise velocity), trapezoidal rule can be used to solve the equation of U_b numerically. i.e. *trapz* command in Matlab.

5.3.3 Meshing

In order to see the effects of mesh resolution a hierarchy of meshes was created. Three uniformly spaced meshes, in all directions, were generated namely: Mesh 1 (coarse), Mesh 1_5 (medium) and Mesh 2 (fine). The resolution of Mesh 1 was refined by a factor of 1.5 in all directions for Mesh 1_5 and similarly by a factor of 2 for Mesh 2. To compute the mesh spacing the dimensionless distances in wall normal and wall parallel directions (stream-wise and span-wise) were used. The u_τ used for spacing computation is taken from the DNS data. Initially the plan was to go for Mesh 3, refinement by factor 4 in all directions, but the total number of mesh points were $\sim$ 88 *million* ,so the idea was dropped and an intermediate mesh resolution was chosen and hence the name Mesh 1_5.

$$\begin{aligned} x^+ &= \frac{\Delta x u\tau}{\nu} \\ y^+ &= \frac{\Delta y u\tau}{\nu} \\ z^+ &= \frac{\Delta z u\tau}{\nu} \end{aligned} \tag{15}$$

Because of the uniform meshes the spacing is same in all three directions and from now onward it will be referred as Δ^+. The bottom and top faces of the domain were defined as the wall, no-slip boundary condition. The no-slip boundary condition was realized by using the half-way bounce back boundary condition. Because of the half-way bounce back boundary condition the distance of the nearest cell to the wall, y^+, is halved [14]. The y^+ will always be a smaller than Δ^+ by a factor of 2. The following table 3 shows the mesh statistics used in the investigation, where N_x , N_y , N_z denote the number of nodes in the stream-wise, wall-normal and span-wise directions. In order to facilitate the grid generator the size of domain was reduced to 6δ x 2δ x 3δ.

	N_x x N_y x N_z	*Total nodes*	$\sim \Delta^+$	$\sim y^+$
Mesh 1	192 x 64 x 96	1179648	12	6
Mesh 1_5	288 x 96 x 144	3981312	8	4
Mesh 2	384 x 128 x 192	9437184	6	3

Table 3: Mesh statistics

The domain size has been slightly altered in this investigation and this leads to the necessity for performing the two-point correlations to prove the adequacy of the domain. *Premnath et.al* [15] suggests doing it otherwise.

5.4 Initial conditions

It is known from the theory of the internal fluid flow that there exists a hydrodynamic entry length (L_h), starting from the inlet (x = 0), that the fluid has to travel, in the channel, for the flow to become fully developed. This means when we integrate the flow governing equations, in time, the fluid has to travel the distance L_h ($\sim x = 10H$) in every time-step, to generate a fully developed flow, which is unnecessary considering the computational efforts and also the storage requirements. The idea is to consider only that portion of the channel which will be fully developed, turbulent and neglecting the initial part (L_h) of the channel. This implies that specific initial conditions for the flow to become fully developed and turbulent has to be provided.
Different approaches have been used by different authors to generate the initial condition for the incompressible, three-dimensional, turbulent channel flow simulations.*Moin et.al* [8] has specified few consistency criteria for initial velocity field. *Sagaut* [16] & *Fröhlich* [4] have a concide description of most commonly used approaches with their respective advantage, disadvantages and their applications to suitable flows. Two of the several approaches mentioned in [16] & [4] will be discussed here.

i. First approach: In this approach a simulation is performed for some Reynolds number smaller than the one to be simulated. The resulting fields of this simulations are then used as the starting point for the required Reynolds number and is simulated further in time until a steady state, where the statistics of the flow do not change with time, is achieved. This approach is termed as *Precursor simulation* in several literature.

ii. Second approach: In this approach a laminar flow is chosen as the base flow and certain set of disturbances are applied on the base flow. The base flow super-imposed with disturbances is then integrated in time until the flow

transitions to a turbulent flow. This approach is computationally intensive, as the flow takes time to become turbulent. There are several options available to impose the disturbances on to the base flow. Several authors have used this approach for the generating appropriate initial conditions. In this investigation this approach has been used.

For the initialisation of our simulations the approach of *Eugene de Villiers* [13] was followed. *Eugene de Villiers* introduced some sort of near wall streak cycle, where he uses the fundamentals of the turbulent structures near the walls. A parabolic flow profile is chosen as the base flow. To generate the parabolic flow profile the bulk mean velocity, $U_b = 0.1335\ m/s$, which was computed by [13], from the mean velocity DNS data of [9] for $Re_\tau = 395$, is used.

Parabolic flow profile has been applied in the stream-wise direction, $u(y, 0)$, on all the fluid nodes in the domain. Figure 5 shows the parabolic profile used as the base flow. A combination of sine and cosine waves have been used to break the flow symmetry and to develop the turbulence in the flow. Initially the the

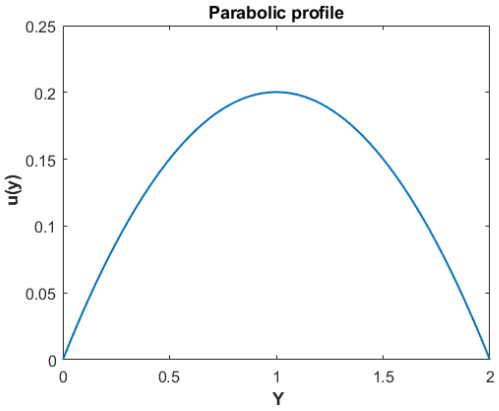

Figure 5: Parabolic flow profile with $U_b = 0.1335\ m/s$

disturbances were applied in the stream-wise direction, but that approach was quite time consuming. It took approximately 4.5 million time-steps for the flow to become turbulent. In the next approach the disturbance was applied in the wall-normal direction, v. This approach reduced the time it took for the flow to becomee turbulent, 100,000 time-steps. The exact equations for the initialization have been specified in the the eq. 18 in Appendix.

5.5 Modelling of pressure gradient

In the theoretical section it was shown that the pressure gradient drives the flow through a channel. With the periodic boundary conditions applied in the both streamwise and spanwise direction no information on the pressure gradient is available and thus some kind of external forcing is required to drive the flow through the channel. This requires an additional step, to model the pressure gradient, in the numerical simulation. An additional force term will be added on the right hand side of the Navier-stokes equation. Forcing is only applied in

the streamwise direction, F_x. Two most commonly used modelling strategies will be discussed here.

i. Constant Pressure gradient :
In this approach we set F_x to some constant value, thus explicitly setting the driving force, which becomes constant and uniform. Since the forcing is constant the mass flow rate will be varying in time, which is attributed to the wall shear stress, until the flow is fully developed (see eq. 4).

$$F_x = -\frac{\partial P}{\partial x} = \frac{\tau_w}{\delta} = \frac{\rho u_\tau^2}{\delta} \tag{16}$$

Thus the simulation a posteriori yields the mean flow rate, U_b, required to generate the prescribed frictional losses [17]. [18, 10] have used this forcing strategy.

ii. Constant Flow rate : In this approach the forcing is not constant, but it is time dependent. The forcing is adjusted in every time step to keep the mass flow rate in the channel equal to the specified flow rate. Flow rate per channel cross-sectional area is U_b. Thus U_b is provided as the input and we get the mean friction velocity, u_τ as the output which we compare with that of the DNS result. This is the most widely used approach in the turbulent channel simulations [13, 11, 19] and it has been utilised in this investigation. Detailed description of this approach is specified rarely and the authors [17, 20] describe the approach in detail. [17] has shown a comparison between different forcing strategies applied on the turbulent channel flow.

5.6 Solver settings

Once the flow in the channel becomes turbulent, the flow is allowed to further develop in time until the it reaches a statistically steady state i.e. the statistics of the flow variables are invariant to temporal changes. Once the velocity field reaches the statistically steady state, the equations are further integrated in time to obtain the time average of the various statistical correlations and these time averaged quantities are further averaged in space along the two homogeneous directions i.e spatial averaging over the x-z planes.

To determine the statistically steady state in the channel one can observe the evolution of the several quantities viz. turbulent kinetic energy (volume averaged), τ_w, u_τ etc. over some non-dimensional time. Refer to [21] for the detailed description for steady state determination and spatial averaging. Here two non-dimensional time will be specified *large-eddy turn-over-time (LETOT)*, tu_τ/δ, and the flow through the domain time, tU_b/δ. The u_τ obtained from DNS data is used for computing the LETOT. LETOT is the time required by the large eddy to breakdown and transfer the energy to the small eddies [12]. In this investigation no specific quantity had been monitored to determine the statistically steady state. An estimation that ~ 10 *LETOT* is sufficient for the flow to be fully developed and statistically steady [22] had been followed.

The lb simulations are generally performed in *lattice units*, where all the physical parameters are represented by dimensionless numbers. This implies that converting the dimensional quantities into dimensionless lattice quantities and vice versa to interpret the simulation results. Exploiting the law of similarity we can ensure that we simulate the same kind of flow in both the unit systems

by maintaining certain non-dimensional parameters equal in both unit systems i.e. Reynolds number.

LB is mostly used for simulating the incompressible fluids where the Mach number is smaller ($Ma < 0.3$). The flow in this investigation is also incompressible. Smaller Mach number $Ma \ll 1$ implies that the flow in the channel evolves with smaller time-step, Δt, i.e. flow evolves slowly and thus renders the simulation as computationally expensive. In order to avoid that, Ma has been artificially increased to speed-up the simulation i.e. coarser Δt by keeping the Re number constant. The computation of the parameters required to increase the Ma is specified in the Appendix. The table 4 shows the actual, Ma_{act}, and the artificial, Ma_{art}, Mach number.

Mach number	Value
Ma_{act}	0.000389213
Ma_{art}	0.180647487

Table 4: Mach number

There are two stages in the simulation of turbulent channel flow: Flow development stage and the averaging stage. In the flow development stage the flow is allowed to develop till it reaches the statistically steady state and in the averaging stage the statistics of the flow variables are sampled. Table 5 shows the time, dimensional and non-dimensional values, required by different mesh resolutions for each stage. As suggested by [22] ~ 10 $LETOT$ is sufficient for

	$\sim time$	Mesh1	Mesh1_5	Mesh2
Flow developing stage	$t\ [s]$	7324	9806	12871
	tu_τ/δ	57	77	101
	tU_b/δ	977	1309	1718
Averaging stage	$t[s]$	65917	76002	69873
	tu_τ/δ	520	600	552
	tU_b/δ	8800	10146	9328

Table 5: Solver settings

the flow development stage, but the table 5 shows some higher values as it also involves the duration over which the flow becomes turbulent. In the averaging stage the averaging was carried out for longer duration to make sure that we have symmetric Reynolds stress component profiles. This decision was made after observing the profiles generated from every temporal and spatial averaged data set. Mean velocity profiles relatively require less time to have a steady symmetric profile.

5.7 Computational details & Post-processing

Simulations have been carried out on the Phoenix cluster [23] of TU Braunschweig. Computations have been performed on the one of the 8 available GPU nodes. Visualisation of the large data sets has been performed using the one

of the 6 available visualisation nodes on the cluster. Time averaging of the flow variables along with the other turbulence statistics is performed during the simulations within the solver itself i.e. running time average as referred in the literature [8]. Spatial averaging is performed a posteriori in Matlab. Paraview together with python scripting is used to manipulate and extract the data from the resulting time-averaged data sets. Paraview is also used for the visualisation of the instantaneous data i.e. velocity contour plots, iso-volumes etc. The data extracted by the python scripts is then used by the Matlab scripts to further manipulate and visualise the data in the form of profile plots i.e mean velocity profiles, Reynolds stresses.

6 Results and discussion

In this section the results of the simulations will be presented and discussed. Two different variations of the LB solver were tested. One with the optimised values of the relaxation parameters [24] and other with the relaxation parameters used as specified in [25]. The results presented in this section are performed with the former variation of the LB solver and the results of the latter variation will just be presented in the Appendix, as the choice of value one for all the parameters is the most stable choice but not accurate enough [24]. Firstly, the results of the LB simulations carried out without any turbulence model will be presented and discussed. The result of the simulations with no-model will be termed as the *under resolved DNS* (UDNS). Under resolved because the resolution is coarser compared to the reference mesh resolution and DNS because no additional modelling is done for turbulence. It will be followed by the discussion of the results from the LB-LES with the WALE model and will be compared with the UDNS and DNS results. Few general comments applicable for all the simulations are:

- The DNS results of [6] , for $Re_\tau = 395$, will be used as a reference for the comparison. The quantities obtained from the DNS data will be referred to as the *target* quantities.
- The results shown here are plotted against the global coordinates, y/δ, and local coordinates, y^+.
- All simulations have been performed using the single precision on GPGPUs.
- The normalised wall distance y^+ used in the profile plots is computed a posteriori for all the simulations.

6.1 UDNS results

To test the accuracy of the turbulent channel flow results from the LB solver, against the DNS data, these simulations have been performed. The physical quantities resulting from the simulations for all meshes are listed in the table (6). The average friction velocity (u_τ) and the Re_τ resulting from the computed u_τ are the important quantities. From now on u_τ represents the average friction velocity. The computed value of u_τ is under-predicted for all the simulations and so is the resulting Re_τ, but the values approach the target u_τ with the increase in the mesh resolution. We know from the definition of u_τ,that u_τ is proportional to the τ_w. Thus, smaller values of the u_τ implies smaller values of τ_w.

Physical quantity	Mesh1	Mesh1_5	Mesh2	Target
$u_\tau,\ m/s$	0.0070	0.0074	0.0076	0.0079
Re_τ	352	371	382	395
$U_c,\ m/s$	0.1565	0.1563	0.1557	0.1591

Table 6: Comparison of the resulting physical quantities

6.1.1 Mean velocity profile

Mean velocity profiles presented here have been averaged in time and space. It is seen from the Fig. (6), the mean velocity profiles for all the meshes over-predict the DNS data. As discussed in the section 5.1.2 the viscous sublayer plays a dominant role on the flow characteristics as higher velocity gradients are present there. Since the viscous sublayer is under-resolved in the simulations, u_τ and eventually the τ_w is under-predicted and as a result we see the different flow characteristics obtained from the simulations i.e. over-predicting velocity profiles in comparison to the DNS data. It is clear that with the better resolution of the viscous sublayer, the correct flow characteristics will be obtained and it is apparent from the Fig. (6) that with the mesh refinement, the velocity profiles approach closer to the DNS data. Velocity profile for mesh3 nearly collapses on to the DNS data. Thus a positive effect of mesh resolution is seen from the mean velocity profile plots.

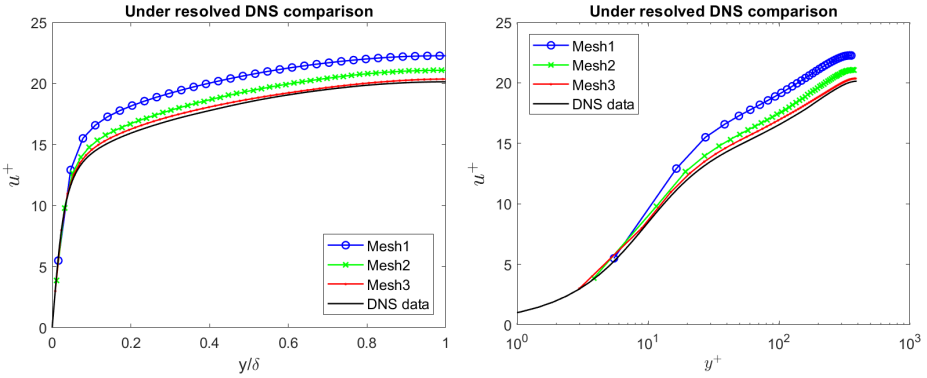

(a) global coordinates (b) wall coordinates

Figure 6: Mean stream-wise velocity profile normalized by u_τ

6.1.2 Turbulence intensities

Turbulence intensities is the term used for the root-mean-square (rms) profiles of the velocity fluctuations. The rms profiles shown in this section have been averaged in the following order: the time-averaged data set written out in every time-step is spatially averaged and these time and space averaged data sets are again time-averaged to have symmetric rms profiles. The Fig. 7 shows the rms velocity fluctuations plotted in the global coordinates. The rms profiles are symmetric about the half-channel height i.e. $y = \delta$ and the symmetry of the profiles about δ indicates the adequacy of the sampling taken for average [6]. Turbulence intensities normalised by u_τ are compared with different mesh resolutions and the DNS data[1].

Fig.(8)-(10) shows the comparison of the components of the rms profiles of the streamwise, wall-normal and spanwise velocity fluctuations, respectively,

[1]the DNS data for the velocity fluctuation profiles have been provided as variances ($\overline{u'^2}$) and not the rms ($\sqrt{\overline{u'^2}}$)values

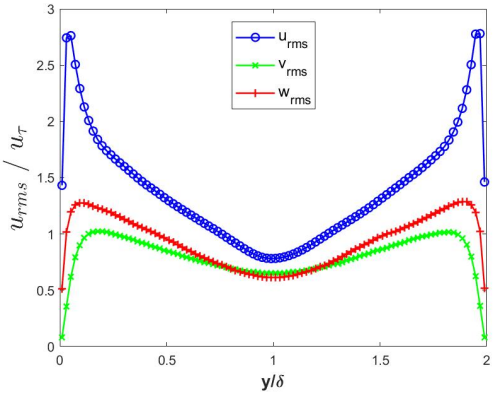

Figure 7: Root-mean-square velocity fluctuations normalized by u_τ in global coordinates

with the different mesh resolutions and the DNS data in wall coordinates. The profiles do not start from zero value, as only the fluid nodes are plotted. The general observation from all three velocity fluctuation profiles is that they converge to the DNS data with the increase in the mesh resolution.

Mesh 2 and Mesh 3 accurately estimates the location of the peak values for all three velocity component profiles, respectively, compared to the DNS data. Mesh 3 for all the velocity component profiles predict the peak value fairly close to that of the DNS data. All three velocity component profiles for Mesh 3 are in fairly good agreement with the DNS data.

The rms value of the streamwise profile increases from zero at the wall to some peak value in either buffer layer, $5 < y^+ < 30$, or in the log-law layer, $y^+ > 30$ *till* $y/\delta < 0.3$ and then drops gradually towards the centre of the channel. The velocity profile for the wall-normal component develops slowly in comparison to the streamwise and the spanwise component profiles. The approximate location of the peak value for streamwise profile (DNS) is at $y^+ = 14$ [6] i.e. buffer layer. The location of peak value for the spanwise component (DNS) is at $y^+ = 40$ i.e. log-law region and the location for the wall-normal component (DNS)is at $y^+ = 70$ also in the log-law region, but towards the end of it. The resulting profiles of Mesh 3 for all components approximately shows the same locations for the peak values as that of the corresponding DNS data.

6.1.3 Turbulent shear stress

Turbulent shear stress is also referred to as the co-variance of the Reynolds stress tensor i.e. $-\overline{u'v'}$. This component is responsible for the turbulent diffusion of the momentum. It is also sometimes referred to as the resolved shear stress.

Fig. (11) shows the turbulent shear stress profile normalised with the u_τ^2 plotted in wall coordinates and compared against the DNS data and with the mesh resolutions. As seen from the Fig. (11) the increase in the mesh resolution results in the better agreement to the DNS data. Mesh 3 here shows a very good agreement to the DNS data and also it predicts the location of the peak value, $y^+ = 35$ fairly well.

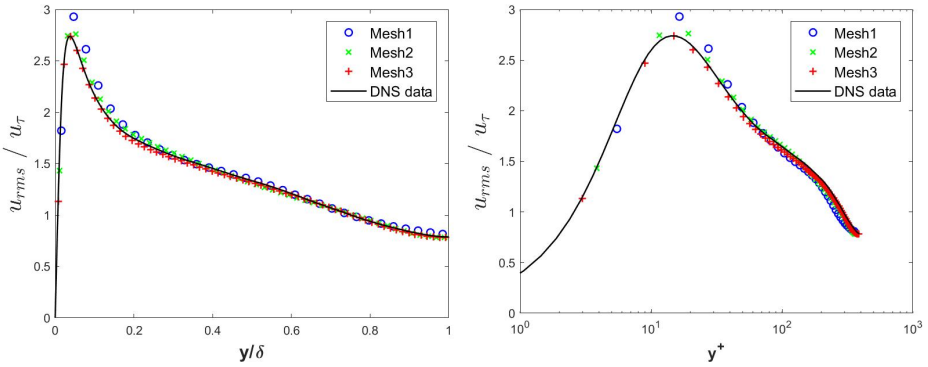

(a) global coordinates (b) wall coordinates

Figure 8: Rms profiles for the streamwise velocity fluctuation normalised by u_τ

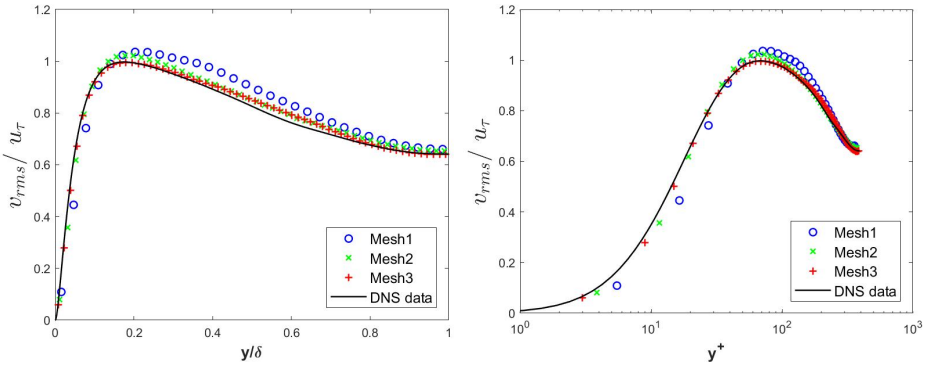

(a) global coordinates (b) wall coordinates

Figure 9: Rms profiles for the wall-normal velocity fluctuation normalised by u_τ

6.2 WALE model results

In this section the results obtained from the combination of the LB flow solver with the WALE model (LES) performed on the relatively coarser mesh, in comparison to the resolution of the DNS data, will be presented. The main purpose is to access the accuracy with which the aforementioned combination reproduces the mean flow profiles and other turbulence statistics when compared to the DNS data. The computed physical quantities have been listed in the table 7 for all mesh resolutions. The same trend is seen for the physical quantities as mentioned in the section 6.1. The physical quantities approach closer to the respective target values with the increase in the mesh resolution.

6.2.1 Mean velocity profiles

The mean velocity profiles, normalised with the u_τ, presented here are averaged in time and space. Fig. (12(a-b)) shows the mean velocity profiles plotted in

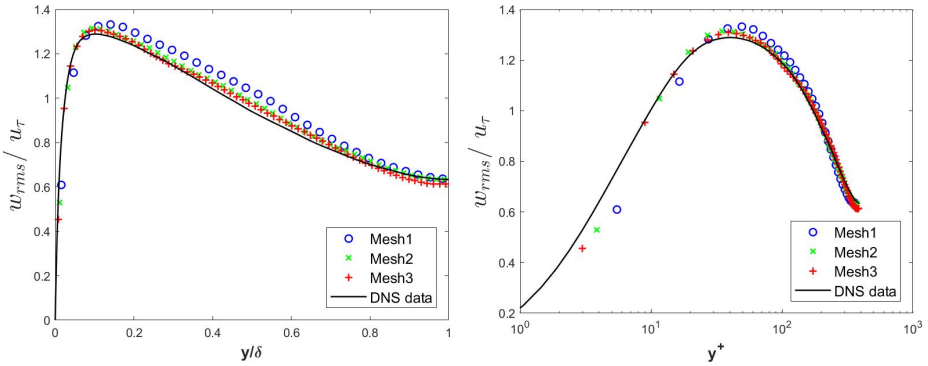

(a) global coordinates (b) wall coordinates

Figure 10: Rms profiles for the spanwise velocity fluctuation normalised by u_τ

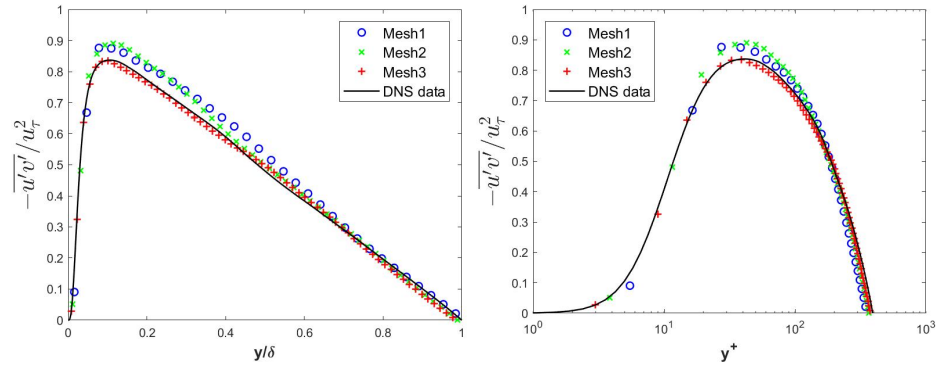

(a) global coordinates (b) wall coordinates

Figure 11: Turbulent shear stress normalised by u_τ^2

Physical quantity	Mesh1	Mesh2	Mesh3	Target
$u_\tau,\ m/s$	0.0069	0.0073	0.0075	0.0079
Re_τ	347	367	377	395
$U_c,\ m/s$	0.1562	0.1557	0.1547	0.1591

Table 7: Comparison of the computed physical quantities using WALE model

the global and local coordinates. It is clear from the both the figures that with increase in the mesh resolution the velocity profiles approach closer to the DNS data. All profiles over-predict the DNS data, but the velocity profile for the mesh 3 is relatively in good agreement with the DNS data. The reason for the over-prediction is similar to that explained in section 6.1.1.

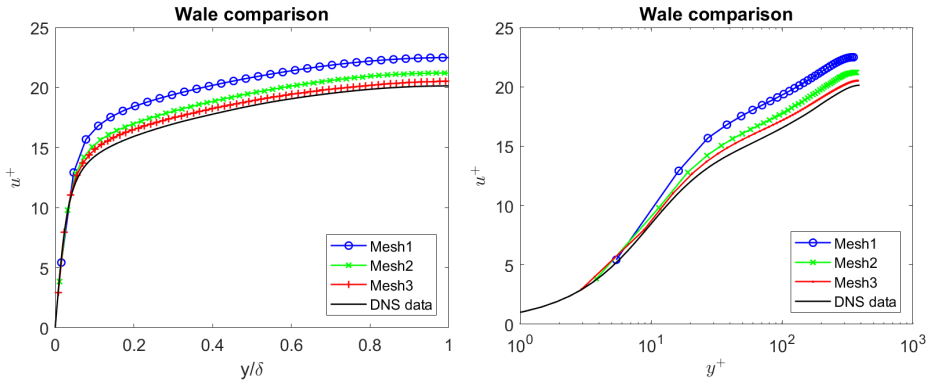

(a) global coordinates (b) wall coordinates

Figure 12: Mean velocity profile normalised with u_τ

6.2.2 Turbulence intensities

The rms profiles presented here are averaged in the same fashion as that of the section 6.1.2. To show the adequacy of sampling taken for averaging the symmetric rms profiles, about the half-channel height $y = \delta$, of all three velocity fluctuations is shown in Fig. (13). The comments made in the section 6.1.2 for the velocity profiles are also applicable here. The rms velocity profiles for all three components show a good agreement towards the DNS data as the mesh resolution increases.

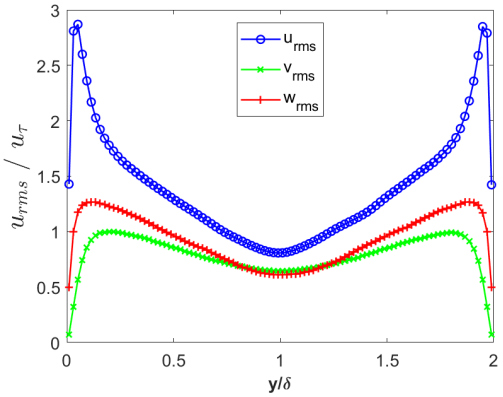

Figure 13: Root-mean-square velocity fluctuations normalized by u_τ in global coordinates

From Fig. (14) it is clear that the location of the peak value is predicted nearly correctly by rms profile of mesh 3. Rms profiles of all meshes overpredict the reference(DNS data) peak value. Overall mesh 3 shows a better agreement to the DNS data, although with a slight overprediction of the peak value.

From Fig. (15) it appears that profile for mesh 1 is shifted towards the right and so is the location of the peak value. With mesh refinement the profiles shift towards the left and the peak value is under-predicted by mesh 1 and mesh 3.

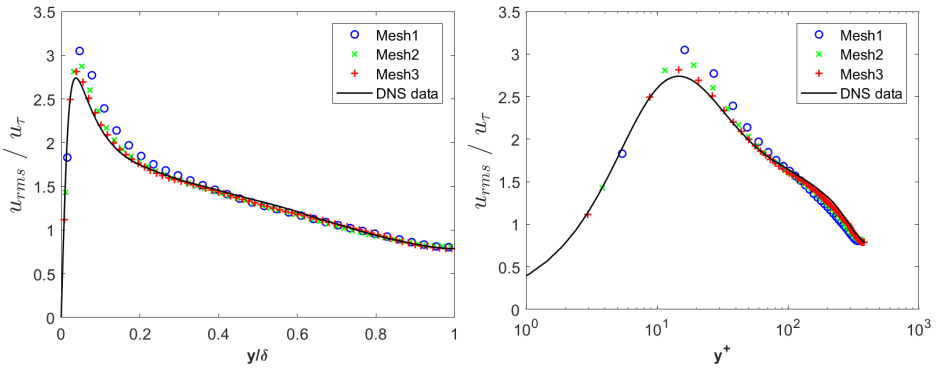

(a) global coordinates (b) local coordinates

Figure 14: Rms profiles for the streamwise velocity fluctuation normalised by u_τ

Mesh 2 somehow overpredicts the peak value. All profiles underpredict in the viscous sublayer (mesh 2 and mesh 3) and the buffer layer. Resolution for mesh 3 approximates the DNS data quite well, although, with some underprediction in the log-law layer i.e. peak value.

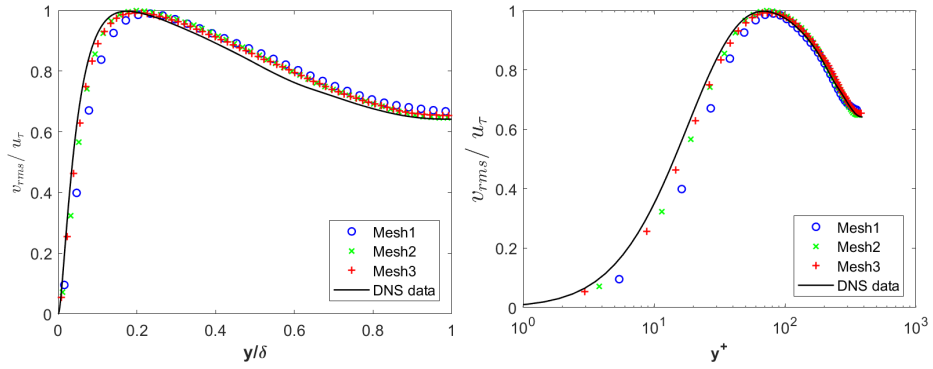

(a) global coordinates (b) local coordinates

Figure 15: Rms profiles for the wall-normal velocity fluctuation normalised by u_τ

Fig. (16) shows that all the profiles overpredict the location of the peak values and also the peak values. Mesh 3 shows a better agreement with the DNS data, with some overprediction in the log-law layer.

6.2.3 Turbulent shear stress

Fig. (17) shows the turbulent shear stress normalised by u_τ^2 plotted in global and wall coordinates. Mesh 1 and mesh 2 overpredicts the DNS data in the log-law layer and eventually the peak value. Profile for mesh 3 completely collapses on to the DNS data.

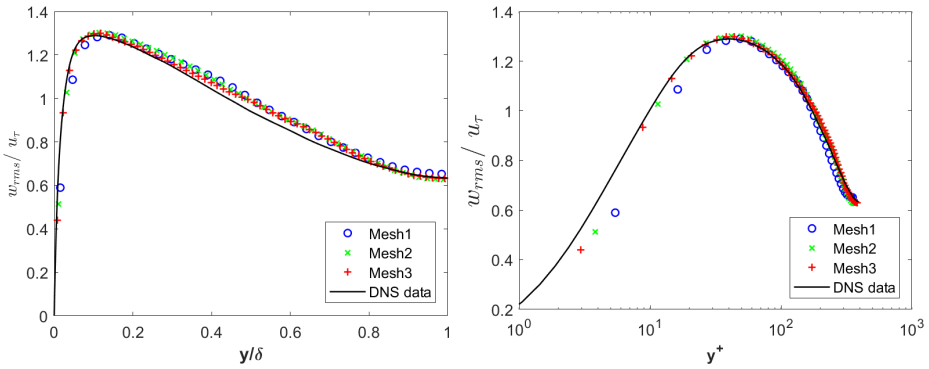

(a) global coordinates (b) local coordinates

Figure 16: Rms profiles for the spanwise velocity fluctuation normalised by u_τ

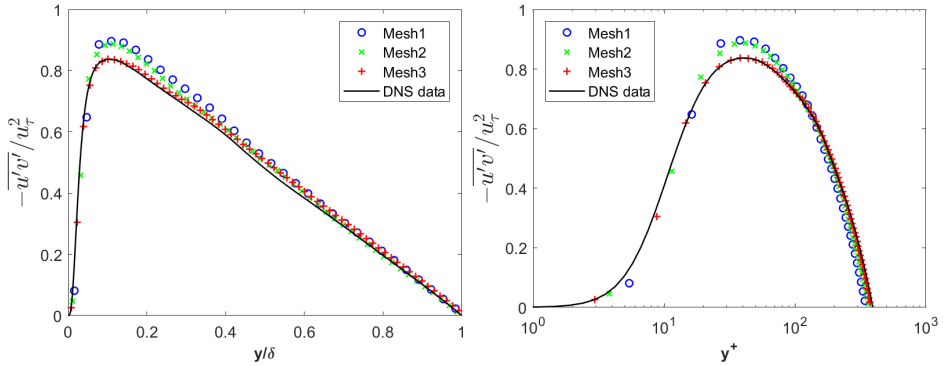

(a) global coordinates (b) local coordinates

Figure 17: Turbulent shear stress profiles normalised by u_τ

6.3 Comparison UDNS and WALE

In this section a comparison will be made between the UDNS and WALE model results. The purpose of this comparison is to see how accurately does the combination of LB solver and WALE model predict the results in comparison to that of the UDNS results. Simultaneously they will also be compared with the DNS data. Only the comparison for the mesh 3 will be shown in here and the comparison for other resolution will be shown in the Appendix. From the table (6) and (7) it can be seen that u_τ and the resulting Re_τ for the WALE model are smaller in comparison with that of the UDNS.

6.3.1 Mean velocity profile

Fig. (18) and Fig. (19) show the comparison of the mean velocity profiles, normalised by u_τ, with the results of UDNS, WALE and the DNS data in global and wall coordinates. Both the profiles overpredict the DNS data. The profile of WALE shows a slight more overprediction in comparison to the UDNS

profile.

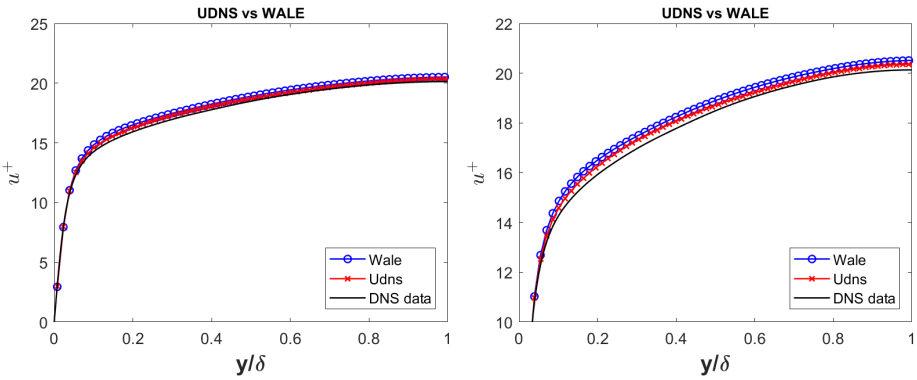

(a) global coordinates (b) zoom in fig. (a)

Figure 18: Mean velocity profiles normalised by u_τ

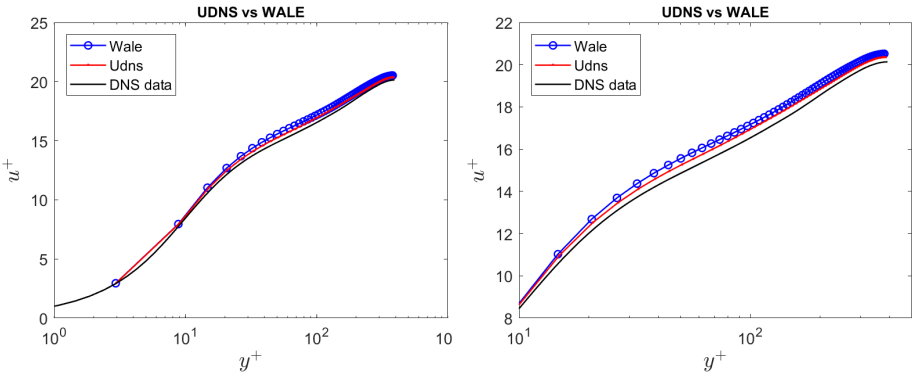

(a) wall coordinates (b) zoom in fig. (a)

Figure 19: Mean velocity profiles normalised by u_τ

The general explanation for the overprediction is the resulting u_τ being smaller, for WALE & UDNS, in comparison to the DNS data. The same applies to the overpredicting profile of the WALE in comparison to the UDNS profile. Ideally, both profiles, WALE & UDNS, should underpredict the reference profile and this behaviour can be seen when we plot just the mean velocity and not the normalised mean velocity, u^+.

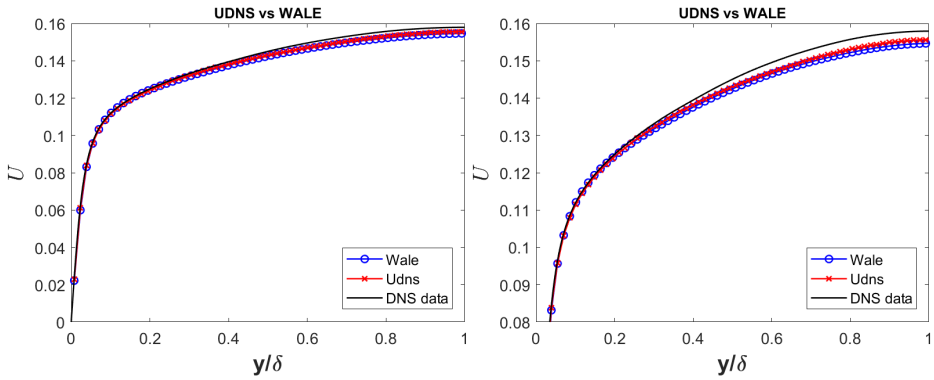

(a) global coordinates (b) zoom in fig. (a)

Figure 20: Mean velocity profiles

A Appendices

A.1 Initial conditions

The following are the initial conditions, for density and the velocity components resp, used for fully developed channel flow simulations:

$$\rho = 27\ U_b^2 \left(cos\,(x)\,\frac{4\pi}{x} + cos\,(y)\,\frac{4\pi}{y} \right) \frac{y}{x} + 27\ U_b^2 \left(cos\,(x)\,\frac{4\pi}{x} + cos\,(z)\,\frac{4\pi}{z} \right) \frac{z}{x} \tag{17}$$

$$\begin{aligned} u &= 3 * U_b \left(\frac{y}{h} - 0.5 \left(\frac{y^2}{h^2} \right) \right) \\ v &= U_b * cos\,(x)\,\frac{2\pi}{x} * sin\,(y)\,\frac{2\pi}{y} \\ w &= 0 \end{aligned} \tag{18}$$

A.2 Lattice units

As mentioned earlier the lattice units are the dimensionless lattice values of the corresponding physical parameters. Chapter 7 in [14] provides the detailed explanation on how to non-dimensionalise and several considerations while performing that to the physical units. For the further discussion the lattice units will be marked with an asterisk, *, sign and the unmarked symbols will represent the physical parameters. As mentioned earlier to simulate the same flow, the Reynolds number in both the unit systems has to be equal. Here the Re_b is taken as the reference.

$$\begin{aligned} Re^* &= Re_b \\ \frac{U^* l^*}{\nu^*} &= \frac{U_b\ l}{\nu} \end{aligned} \tag{19}$$

The total number of grid nodes are same in both unit system, thus :

$$\begin{aligned} N^* &= N \\ \frac{l^*}{\Delta x^*} &= \frac{l}{\Delta x} \\ l^* &= \frac{l}{\Delta x} \Delta x^* \end{aligned} \tag{20}$$

The usage of the uniform grid here implies that $\Delta x^* = 1$. With the same assumption as of Reynolds number the lattice and the physical Mach number must also match and this implies:

$$\begin{aligned} Ma^* &= Ma \\ \frac{U^*}{{c_s}^*} &= \frac{U_b}{c_s} \\ U^* &= Ma\ {c_s}^* \end{aligned} \tag{21}$$

where c_s^* is the lattice speed of sound and equal to $\frac{1}{\sqrt{3}} \approx 0.577$. When simulating the incompressible flow simulations the Mach number is small and hence it is not necessary to equate the Mach number until and unless it is small. Mach number is lattice units is considered small when $Ma^* < 0.3$ [14]. Now l^* and U^* are known the only free parameter ν^* can be computed by using the eq. 19.

As mentioned before the Mach number of the simulation is very small i.e. $Ma \ll 1$, as the flow is incompressible. This means that the U^* will be very small and thus Δt which scales as $\Delta t \propto Ma^*$ will also be very small. The total simulation time, T, is expressed as [14]

$$T \propto \frac{1}{\Delta x^n \Delta t}$$

where n is the spatial dimension. This shows that smaller Δt requires a large number of time-steps for the flow to develop. Hence it is suggested to some how increase Ma^* and eventually U^* as $U^* \propto Ma^*$. Let us consider an example of Mesh 1 resolution to show how the Mach number was increased.

$$\begin{aligned} U^* &= \frac{Re_b \nu^*}{l^*} \\ Ma^* &= U^* \sqrt{3} \end{aligned} \tag{22}$$

$l^* = 64$ and ν^* is chosen equal to 0.0005 and the resulting $U^* = 0.104296875$. With the increase in the mesh resolution the ν^* also increases to keep the Reynolds number same. Thus the eq. 22 show how the Ma^* has been increased. The intrinsic restrictions of LB algorithm however puts a limit on the simulation parameters i.e. Ma^* [14]. Thus there is a upperlimit till which the Ma^* can be increased. The table 8 shows the parameters in lattice units to increase the Mach number.

	Mesh1	Mesh1_5	Mesh2
U^*	0.104296875	0.104296875	0.104296875
ν^*	0.0005	0.00075	0.001
l^*	64	96	128

Table 8: Parameters in lattice units

References

[1] Y.A. Cengel and J.M. Cimbala. *Fluid Mechanics: Fundamentals and Applications*. McGraw-Hill, New Delhi, 2 edition, 2011.

[2] P.K. Kundu and I.M. Cohen. *Fluid Mechanics*. Academic Press, 525 B Streek Suite 1900, San Diego, California 92101-4495, USA, 2002.

[3] S.B. Pope. *Turbulent Flow*. Cambridge University Press, Cambridge, UK, 2001.

[4] Jochen Fröhlich. *Large Eddy Simulationen turbulenter Strömungen*. Teubner/GWV Fachverlage GmbH, Wiesbaden, DE, 2006.

[5] http://turbulence.ices.utexas.edu/.

[6] J. Kim, P. Moin, and R. Moser. Turbulence statistics in fully developed channel flow at low Reynolds number. *Journal of Fluid Mechanics*, 177:133–166, 1987.

[7] Myoungkyu Lee and Robert D. Moser. Direct numerical simulation of turbulent channel flow up to $Re_\tau \approx 5200$. *Journal of Fluid Mechanics*, 774:395–415, 2015.

[8] P.Moin, W.C. Reynolds, and J.H.Ferziger. Large eddy simulation of incompressible turbulent channel flow. Technical report number t-12, Thermosciences Division, Department of Mechanical Engineering, Stanford University, Stanford, California, 1978.

[9] R.D. Moser, J.D. Kim, and N.N. Mansour. Direct numerical simulation of turbulent channel flow up to $Re_\tau = 590$. *Physics of Fluids*, 11:943–945, 1999.

[10] R.K. Freitas, A. Henze, M. Meinke, and W. Schröder. Analysis of lattice-boltzmann methods for internal flows. *Computers and Fluids, Elsevier*, 47:115–121, 2011.

[11] S. Uphoff. *Development and Validation of turbulence models for Lattice Boltzmann schemes*. PhD thesis, TU Braunschweig, Fakultät Architektur, Bauingenieurwesen und Umweltwissenschaften, Braunschweig, Germany, 2012.

[12] D.J. Bespalko. *Validation of the Lattice Boltzmann Method for Direct Numerical Simulation of Wall-Bounded Turbulent Flows*. PhD thesis, Queen's University, Department of Mechanical and Materials Engineering, Canada, 2011.

[13] Eugene de Villiers. *The Potential of Large Eddy Simulation for the Modeling of Wall Bounded Flows*. PhD thesis, Thermofluids Section, Department of Mechanical Engineering, Imperial College of Science, Technology and Medicine, Kensington, London SW7 2AZ, 2006.

[14] T. Krüger, H. Kusumaatmaja, A. Kuzmin, O. Shardt, G. Silva, and E.M. Viggen. *The Lattice Boltzmann Method: Principles and Practice*. Springer, Cham, Switzerland, 2016.

[15] K. Premnath, M.J. Pattinson, and S. Banerjee. Generalized lattice-boltzmann equation with forcing term for computation of wall- bounded turbulent flows. *Computational Physics*, 2009.

[16] P. Sagaut. *Large Eddy Simulation for Incompressible Flow*. Springer Verlag, 2002.

[17] Maurizio Quadrioa, Bettina Frohnapfel, and Yosuke Hasegawa. Does the choice of the forcing term affect flow statistics in dns of turbulent channel flow? *Cornell university library*, 47:115–121, 2015.

[18] K. Premnath, M.J. Pattinson, and S. Banerjee. Dynamic subgrid scale modeling of turbulent flows using lattice-boltzmann method. *Computational Physics*, 2009.

[19] David Roos Launchbury. *Unsteady Turbulent Flow Modelling and Applications*. Springer Vieweg, Wiesbaden, 2016.

[20] E. Lenormanda, P. Sagaut, and L. Ta Phuoc. Large eddy simulation of subsonic and supersonic channel flow at moderate reynolds number. *INTERNATIONAL JOURNAL FOR NUMERICAL METHODS IN FLUIDS*, 32:392–406, 2000.

[21] Javier Jiménez and Parviz Moin. The minimal flow unit in near-wall turbulence. *Journal of Fluid Mechanics*, 225:213–240, 1991.

[22] Prof. Manfred Krafczyk. personal discussion.

[23] https://www.tu-braunschweig.de/it/dienste/21/phoenix.

[24] Martin Geier, Andrea Pasquali, and Martin Schönherr. Parametrization of the cumulant lattice boltzmann method for fourth order accurate diffusion part i: derivation and validation. *Journal of Computational Physics*, 348:862–888, 2017.

[25] Martin Geier, Martin Schönherr, Andrea Pasquali, and Manfred Krafczyk. The cumulant lattice boltzmann equation in three dimensions: Theory and validation. *Computers and Mathematics with Applications*, 70:507–547, 2015.